CORA Cork Open Research Archive
Cartlann Taighde Oscailte Chorcaí

Title	Metal catalyzed porous n-type GaN layers: low resistivity ohmic contacting and single-step MgO/GaN diode formation
Authors	Bilousov, Oleksandr V.;Carvajal, Joan J.;Drouin, Dominique;Vilalta, A.;Ruterana, P.;Pujol, M. C.;Mateos, X.;Diaz, Francesc;Aguilo, Magdalena;O'Dwyer, Colm
Publication date	2013-04
Original Citation	Bilousov, O. V., Carvajal, J. J., Drouin, D., Vilalta, A., Ruterana, P., Pujol, M. C., Mateos, X., Díaz, F., Aguiló, M. and O'Dwyer, C. (2013) 'Metal Catalyzed Porous n-type GaN Layers: Low Resistivity Ohmic Contacting and Single-Step MgO/GaN Diode Formation', ECS Transactions, 53(2), pp. 17-27. doi: 10.1149/05302.0017ecst
Type of publication	Article (peer-reviewed)
Link to publisher's version	10.1149/05302.0017ecst
Rights	© 2013 ECS - The Electrochemical Society
Download date	2024-10-09 07:28:48
Item downloaded from	https://hdl.handle.net/10468/6132

UCC
University College Cork, Ireland
Coláiste na hOllscoile Corcaigh

Metal catalyzed porous n-type GaN layers: low resistivity ohmic contacting and single-step MgO/GaN diode formation

O. V. Bilousov[1], J. J. Carvajal[1], D. Drouin[2], A. Vilalta[3], P. Ruterana[3], M. C. Pujol[1], X. Mateos[1], F. Díaz[1], M. Aguiló[1], C. O'Dwyer[4,5]

[1] *Physics and Crystallography of Materials and Nanomaterials (FiCMA-FiCNA), Universitat Rovira i Virgili (URV), Tarragona, Spain*
[2] *Department of Electrical and Computer Engineering, Université de Sherbrooke, Sherbrooke, Québec J1K 2R1, Canada*
[3] *CIMAP, UMR 6252, CNRS-ENSICAEN-CEA-UCBN, 6, Boulevard du Maréchal Juin, 14050 Caen Cedex, France*
[4] *Department of Chemistry, University College Cork, Cork, Ireland*
[5] *Micro- and Nanoelectronics Centre, Tyndall National Institute, Lee Maltings, Cork, Ireland*

Porous GaN crystals have been successfully grown and electrically contacted simultaneously on Pt- and Au-coated silicon substrates as porous crystals and as porous layers. By the direct reaction of metallic Ga and NH_3 gas through chemical vapor deposition, intermetallic metal-Ga alloys form at the GaN-metal interface, allowing vapour-solid-solid seeding and subsequent growth of porous GaN. Current-voltage and capacitance-voltage measurements confirm that the intermetallic seed layers prevent interface oxidation and give a high-quality reduced workfunction contact that allows exceptionally low contact resistivity. Additionally, the simultaneous formation of a lower workfunction intermetallic permits ohmic electron transport to n-type GaN grown using high workfunction metals that best catalyze the formation of porous GaN layers and may be employed to seed and ohmically contact a range of III-N compounds and alloys for broadband absorption and emission. Additionally, we show how a porous GaN rectifying diode can be formed by oxidatively crystallizing Mg typically employed for p-doping GaN, as a layer formed under porous structure resulting in a high-k polycrystalline MgO dielectric.

Introduction

Gallium nitride (GaN) is considered one of the most important wide band-gap semiconductors for a number of applications in electronics and optoelectronics (1). In its porous form, GaN has received particular interest in the last decade due to beneficial optical and electronic properties for gas sensors with high sensitivity (2), and light-emitting diodes (LEDs) with high light extraction efficiency (3). Porous GaN has been typically fabricated by (photo)electrochemical and chemical etching methods (4-7), giving textured surfaces as a result of pore coalescence and variations in etch rates for extended etching times.

We produced porous GaN through the direct reaction of metallic Ga with NH_3 in a simple chemical vapor deposition (CVD) system. Metal catalysts are typically used

to initiate growth through either a vapour-liquid-solid (VLS) (8) or vapor-solid-solid (VSS) (9) mechanism when using molecular beam epitaxy (MBE) and chemical vapor deposition (CVD), where the catalyst can influence the growth, e.g. colloidal gold nanoparticles can initiate the growth of GaN nanowires. Using this procedure we have been able to deposit micrometer size nanoporous GaN particles directly onto boron nitride (BN) (10) and silicon (11) substrates without necessitating any secondary etching or chemical treatment after growth to induce porosity. Furthermore, by using this technique we have demonstrated that it is possible to deposit porous GaN directly onto Si substrates in a single growth step (12). The only requirement, when depositing such porous particles on silicon substrates is that it is necessary to use a metal catalyst to induce the crystal growth of GaN.

The development of porous GaN augers well for new electronic and optoelectronic devices with improved external quantum efficiencies, the incorporation of phosphors for LEDs, and high surface area sensing. However, the electrical properties of porous GaN and their correlation to its growth, have been scarcely reported in the literature.

In this paper, we report the successful growth and simultaneous electrical contacting of nanoporous GaN grown using high work-function Au- and Pt-coated silicon substrates, through the direct reaction of Ga and NH_3 in the CVD system. Au and Pt acted both as catalyst for the synthesis of porous GaN and as electrodes for the electrical characterization of the porous layers. The electrical measurements demonstrate the influence of the growth mechanism so that near-ohmic contacts can be made to n-type porous GaN layers using high work-function metals (Au and Pt) which also form intermetallic seed layers to support vapor-solid-solid (VSS) growth of the porous GaN crystals. Lastly, p-type Mg dopants were deposited in such a way as to seed a Mg film under the porous GaN, which was oxidatively crystallized without changing the dopant type from n- to p-type, resulting in a single step top-down n-GaN/high-k poly-MgO diode.

Experimental

Synthesis of porous GaN particles

Nanoporous GaN microparticles were deposited on Au- and Pt-coated silicon (100) substrates with an area of 1 cm^2, using a horizontal single zone split tubular furnace Thermolyne 79300. Gallium metal (99.99%) and ammonia (>99.98%) were used as the Ga and N sources, respectively. A 20 nm layer of Au or Pt was deposited on the Si substrates using a RF sputtering process (AJA International) at a power of 150 W and a pressure of 3 mTorr. The coated substrate was then placed 2 cm above the Ga source. The quartz tube of the furnace was degassed to a vacuum pressure of 1×10^{-2} Torr, after which NH_3 was introduced through a mass-flow controller at a flow rate of 75 sccm and the furnace heated to the reaction temperature of 1203 K at a rate of 100 K min^{-1}, while the pressure was kept at 15 Torr. The reaction was continued at this temperature and pressure for 60 min under a constant flow of NH_3. Growth was halted by cooling to room temperature without NH_3 flow, reducing the pressure to 1×10^{-2} Torr.

Nanoporous GaN doped with Mg was grown as micron-sized particles by the direct reaction of metallic Ga with ammonia in a tubular CVD system, using gallium metal (99.99%), ammonia (>99.98%) and Mg_3N_2 (99.5%) as the Ga, N and Mg sources, respectively. The Mg_3N_2 powder, with a 0.025 to 1 weight ratio respect to Ga, was placed 5 cm up-stream of the Ga source.

Structural and morphological characterization

X-ray diffraction (XRD) spectra and imaging in θ-2θ geometry of the as-grown sample were made using Cu Kα radiation in a Bruker-AXS D8-Discover diffractometer equipped with parallel incident beam (Göbel mirror), vertical θ-θ goniometer, XYZ motorized stage and a General Area Diffraction Detection System (GADDS) HI-STAR detector with a multiwire proportional counter of area 30 × 30 cm and 1024 × 1024 pixel density. Samples were placed directly on the sample holder and the area of interest was selected with the aid of a video-laser focusing system. An X-ray collimator system allows to analyze areas of 500μm. The X-ray diffractometer was operated at 40 kV and 40 mA to generate Cu Kα radiation. We collected 2D XRD patterns covering a range of 2θ between 20 - 85º at a distance of 15 cm from the sample. The exposure time was 120 s per frame. Identification of the crystalline phases was achieved by comparison of the XRD diffractogram with the ICDD database using Diffrac^{plus} Evaluation software (Bruker 2007).

The nanoporous GaN microparticles deposited on the Si substrates as a porous layer were characterized morphologically using a JEOL JSM 6400 scanning electron microscope (SEM). Before observation samples were coated with a thin layer of gold with a Bal-Tec SCD004 sputterer.

Electrical characterization

Charge transport measurements through the porous GaN films were conducted using 2- and 4-probe measurements using a dc-voltage course and an Agilent 34401A Digital Multimeter in a Peltier cell, thermostated to 295 K in a Faraday cage. Liquid metal contacts were made using In-Ga eutectic blown into a sphere from a gold metallized short borosilicate capillary tube ensuring good wetting (several μm^2) to the rough top-surface morphology of the porous GaN and avoid electrical shorting to the underlying metallized silicon. Measurements were made in 2- and 4-probe arrangements. Resistivity values were extracted from *I-V* curves in the high bias regime (series resistance) and also from 4-point probe measurements. Diode measurements of the GaN/MgO system were made in vertical 2-probe measurements.

Results and Discussion

Vapor-solid-solid growth of porous GaN

Figures 1(a) and (b) confirm that the porous GaN particles have a characteristic morphology consisting of faceted hourglass crystals with a mean size of ~1.5 μm. Crystal growth occurs progressively on the surface with individual crystals ripening until a layer of porous GaN microparticles covers the surface as a porous layer. The GaN layers are both microporous and mesoporous. The microporosity stems from the free space between particles (see Figure 2 (c)), whereas the nanoscale mesoporosity comes from internal pore features within the particles, confirmed with time-resolved focused ion beam (FIB) based tomography (11). The particles obtained on the Si substrates coated with Pt showed a higher degree of internal porosity than those grown from Au-coated Si substrates.

The growth of these GaN nanoporous particles is assisted by a solid particle through the vapour-solid-solid (VSS) mechanism, the main stages of which are: the Ga incorporation into the Au or Pt solid phase eutectic, the formation of a Ga-Au or Ga-Pt alloy, the solubilization of nitrogen in the Ga-Au(Pt) alloy, and finally the nucleation

and growth of GaN (see Fig. 1). HRETM analysis of such structure shows that they are single crystal in nature, with structure defect comprising internal pores within the crystals.

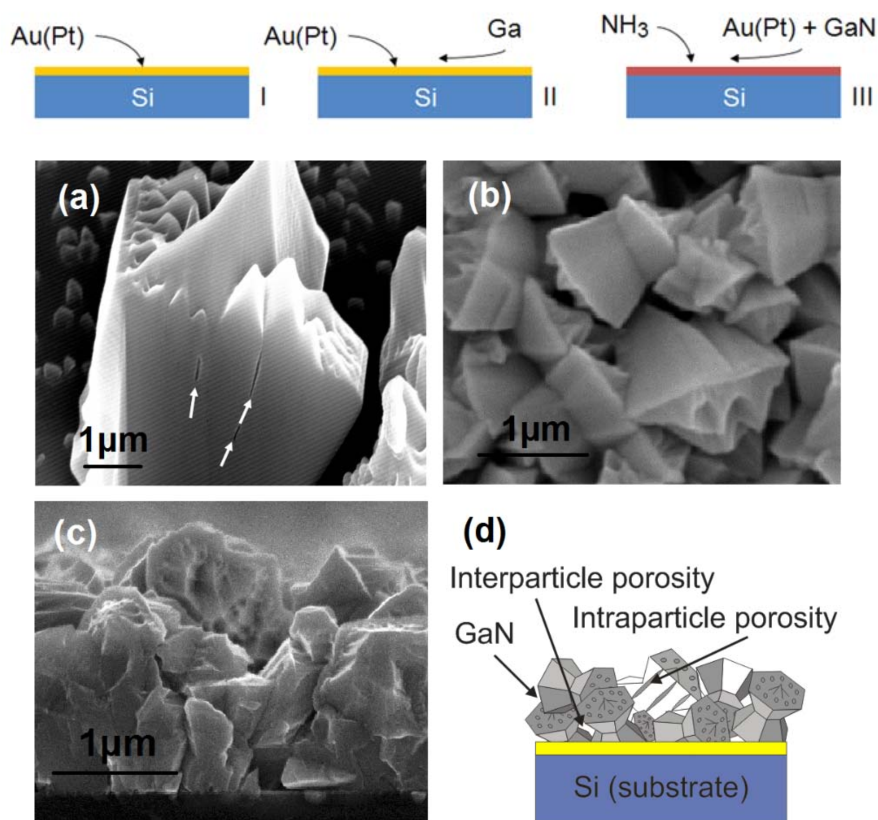

Figure 1. (Top) Mechanism of growth of the GaN nanoporous particles through the VSS process. SEM image of porous GaN particles grown on Si (100) substrates coated with (a) 20 nm film of Au and (b) 20 nm film of Pt. (c) SEM cross sections showing interparticle porosity of the GaN layer. (d) Schematic of the porosity inherent in the GaN film.

The crystalline structure of the porous GaN particles deposited on Si substrates coated with Au and Pt was analysed using X-ray diffraction. The XRD pattern shown in Fig. 2(a) for GaN grown on Au-coated Si substrates, confirms crystalline wurtzite GaN growth with a predominant diffraction intensity from low-index crystal facets. The regions at which the (400) diffraction peak of Si should appear (69.131º) has been excluded from the measurement to avoid problems of intensity saturation. This allows observation of lower intensity reflections that are attributed to crystalline Si_3N_4 and a crystalline Au-Ga intermetallic alloy of cubic Ga_2Au. We believe that the Si_3N_4 formation is most likely due to the reaction between NH_3 and silicon accelerated by the metallic catalyst.

The formation of the Au-Ga crystalline alloy, which occurs here above the solid-solution formation temperature of 923 K, confirms intermetallic seeding to form GaN by reaction with NH_3 through a vapor-solid-solid process. The uniform intensity of the Debye rings (along the curved ring portions in Fig. 2b) collected for porous GaN confirms that there is no texturation of the layer of porous crystals (see Figure 2 (b)). For porous GaN grown on Pt-coated substrates, similar results were obtained, although we could not identify the formation of any specific crystalline Pt-Ga alloy.

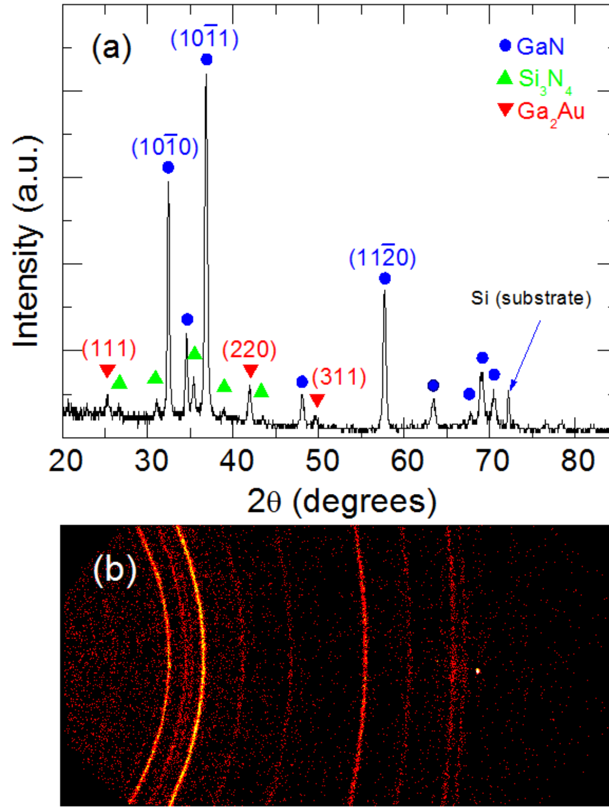

Figure 2. (a) XRD pattern for porous GaN deposited on Au-coated Si(100) showing the formation of crystalline GaN (ICDD 01-073-7289), Si_3N_4 (ICDD 03-065-8613) and Ga_2Au alloy (ICDD 01-071-6479). (b) Debye rings recorded with GADDS detector indicating no texturation of the porous GaN layer.

Electrical characterization of Pt- and Au-contacted porous GaN

Figure 3 shows the *I-V* curves from the porous GaN catalyzed by Pt (Figure 3a) and also by Au (Fig. 4b), with the second contact placed on the underlying metal which was under heating to 1203 K in NH_3. The *I-V* curves show only slight asymmetry indicative of near ohmic, weak Schottky barriers of Pt and Au. Consistently, the conductivity of porous GaN grown from Pt is higher than that grown from Au, in spite of the higher workfunction. The *I-V* curve of porous GaN-Pt in Fig. 4(b) shows the low-bias non-linearity consistent with a weak Schottky barrier. Both contacts are described using the thermionic emission theory, acknowledging a high ideality factor for weak barriers. The Schottky barrier height can still be estimated from:

$$I = I_0\left[\exp\left(\frac{qV - IR_S}{kT}\right) - 1\right] \quad (1)$$

where $I_0 = AA^{**}T^2\exp(-q\varphi^{o}_{B,n}/kT)$[15] where A** is the effective Richardson constant. The estimated Schottky barrier heights using the theoretical value for the effective Richardson constant (26.4 A cm^{-2} K^{-2}) for Pt and Au contacted porous GaN are 0.66 eV and 0.53 eV, respectively.

In spite of the higher porosity from Pt-grown porous GaN, the contact resistivity of the Pt contact is $2 - 4 \times 10^{-4}$ Ω cm^2 while that of the gold contact is $6 - 9 \times 10^{-4}$ Ω cm^2. Thus the interface dominated the transport more than the crystallinity or

morphology of the porous microstructure, and effective ohmic contacts can form with n-type GaN.

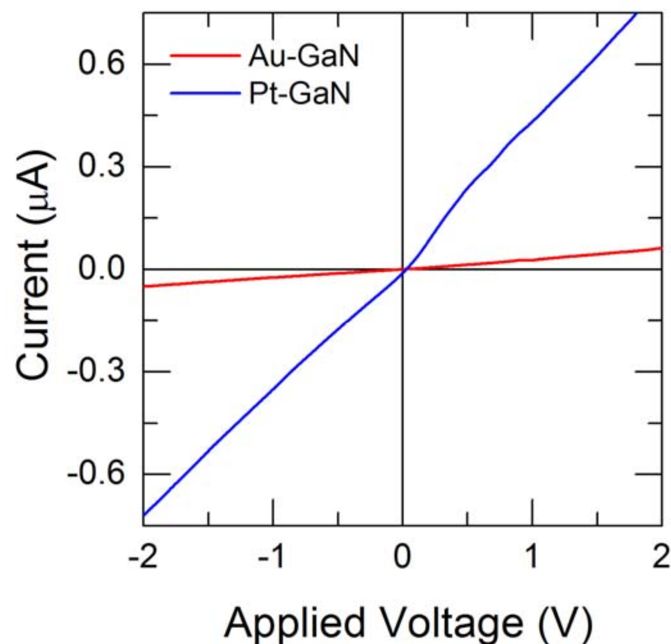

Figure 3. *I−V* curves for porous GaN grown from (a) Pt and (b) Au.

Two terminal transport measurements (Fig. 4a) acquired between the In-Ga ohmic contacts showed perfect ohmicity for transport through the porous GaN layer only, from which low contact resistivities were determined with variable intercontact separation using the TLM approach and found to be in the range 1.7 – 4.4 × 10^{-4} Ω cm^2, in spite of the multifaceted, porous morphology. Corresponding 4-probe analysis gives sheet resistances for porous GaN films in the range 43-49 kΩ/□, which is higher than compact thin film forms as expected from a layer comprising microcrystals in intimate contact. The values, that match those of MBE grown GaN thin films with Ti/Au alloy contacts after annealing to 973 K (16), are caused by the efficient interface between the metal and the growing porous GaN (10). Additionally, although annealing at 1173 K is known to initial improve contact resistivities down to the 10^{-6} Ω cm^2 with Ti/Al contacts, continued heating at this temperature for more than 40 seconds results in a drastic increase in contact resistance (16). The present method avoids this by the use of noble metal contacts as catalysts for the GaN growth. It is worth noting that the n-type contacts were effectively ohmic as deposited and did not need any post-deposition annealing to induce this effective ohmicity; such linear I−V behavior is not found with Au contacts, and the intermetallic seed layer interface is critical for removing the transport Schottky barrier (17).

For the low resistance contacts to a porous GaN layer either a low barrier Schottky contact forms with a graded band-gap interface or a tunnel contact is formed. From XRD analysis, a crystalline Si_3N_4 dielectric layer forms when deposition is performed on silicon, just prior to continued VSS porous GaN growth and is not likely from N out-diffusion from the GaN. The GaN too, is not expected to decompose at 1203 K in NH_3 (it would at a slightly higher temperature in vacuum)[17], but the Au and Pt melting points are close to this temperature. These metals solidify once the crystalline intermetallic Ga_2Au solid phase is formed. Oxide growth that would increase the resistivity of the contact is also prevented.

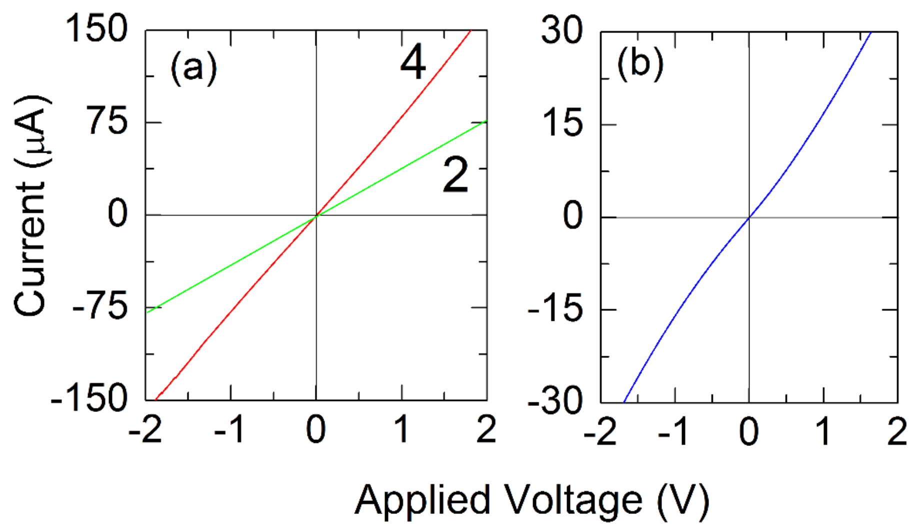

Figure 4. (a) *I*–*V* curve for the porous GaN grown directly from Pt and (c) I–V curves from two- and four-probe measurements using In–Ga ohmic contacts to porous GaN.

The intermetallic Ga_2Au phase suggests a band structure that promotes transport by lowering the Schottky barrier, rather than forming a definitive tunnel contact which shows ohmicity over a small potential range. The intermetallic formation at the interface that allows the growth of the GaN effectively acts as an intermetallic ohmic contact at the semiconductor interface, and the method may be extended to growing nanoscale III-N materials and alloys using metals that are not typically employed for contacting, to give ohmic response.

Single step high-k MgO/porous n-GaN diode formation

When doping these nanoporous GaN with a high concentration of Mg using Mg_3N_2 as precursor, a layer of crystalline MgO is formed in between the Au- or Pt-electrode and nanoporous GaN. Fig. 5 shows the XRD pattern for the resulting deposition.

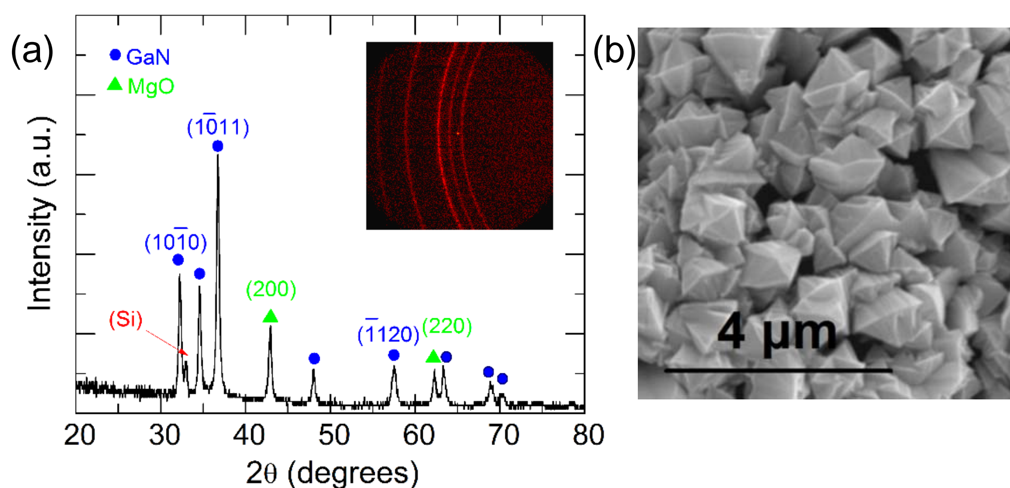

Figure 5. (a) XRD pattern for porous crystalline wurtzite GaN (P63*mc*) doped with Mg grown on a Si(100) substrate using $Ni(NO_3)_2$ as catalyst, with inset of Debye rings. (b) SEM images of the Mg-GaN particles deposited on Si.

We find that deposit also contains crystalline MgO, oxidatively crystallized from the Mg presence during incorporation at the growth stage of the porous GaN. From Fig. 5b, that the single crystals remain nearly identical those grown in the absence of the Mg precursor, and separate data shows that they also retain their unintentionally n-doped character.

TEM analysis confirms that the polycrystalline MgO is located under the porous GaN, in spite of being present at initial stages of the seeding mediated growth of the GaN itself. The high quantities of the Mg-containing precursors preferentially forms this layer rather than doping the GaN lattice. The Mg concentration from TEM energy dispersive X-ray analysis, shown in Fig. 6, confirms the interfacial location of the MgO between the silicon substrate/intermetallic seed layer, and the porous GaN.

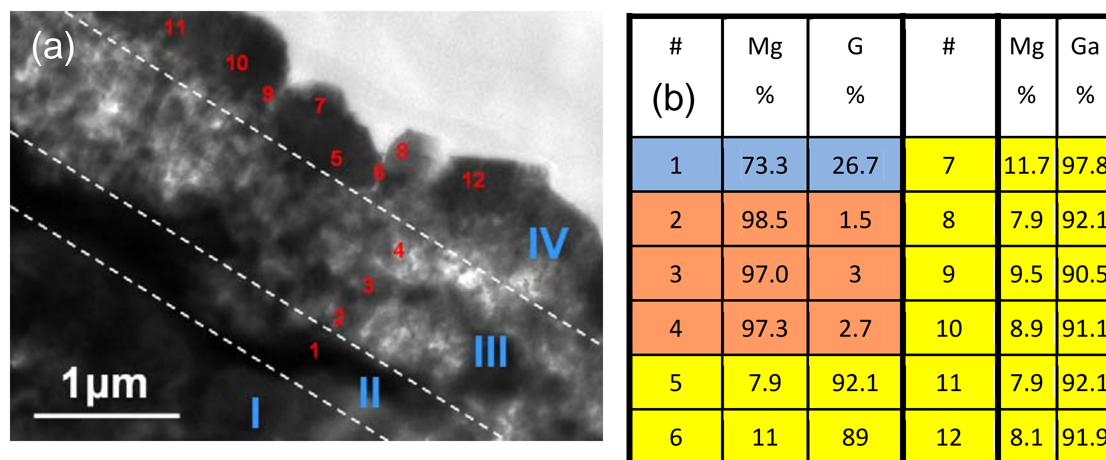

# (b)	Mg %	G %	#	Mg %	Ga %
1	73.3	26.7	7	11.7	97.8
2	98.5	1.5	8	7.9	92.1
3	97.0	3	9	9.5	90.5
4	97.3	2.7	10	8.9	91.1
5	7.9	92.1	11	7.9	92.1
6	11	89	12	8.1	91.9

Figure 6. (a) TEM image of porous GaN layer doped with Mg grown on a Si(100) substrate. (b) EDX content of Mg and Ga in the pores particles. The measurement points (#) relate to those numbered in (a).

Figure 7 shows *I-V* curves across the device using an In-Ga euctectic to ohmically contact both the substrate and the porous GaN. The GaN layer in this case was grown using a Au seed layer. A rectifying diode response is found in the presence of the MgO, compared to ohmic response between the intermetallic termination porous n-GaN and the substrate (18,19). We assumed that the net current is due to thermionic emission current since the metal-semiconductor-metal contact now contains a dielectric at one interface, mimicking a Schottky contact with series resistance and an interfacial layer. Additionally, this is confirmed by forward bias voltages of $V > 3kT/q$, which is the case here. The downturn to linearity in the current after ~0.25 V confirms a series resistance, R_S most likely originates from the MgO and porous n-GaN, as opposed to either of the metal contacts which are confirms to be ohmic in nature. At higher bias (>0.25 V), the R_S dominates, as can be seen from the differential conductance dI/dV curve in Fig. 7a.

Effective ohmic contacts can form with n-type GaN, as shown earlier, suggesting that the resistivity dominates transport through an alloyed interface that promotes ohmic transport. When and high-k MgO layer is introduced, the series resistance markedly increases at much lower voltages. The MgO/n-GaN sandwich effectively has an altered electron affinity with respect to the contact In-Ga top contact.

The overall series resistance, R_S, to which the sheet and contact resistivities contribute can also be determined from diffusion and thermionic emission theory summarised for a Schottky type diode in Eq. (1). In the presence of the intermetallic bottom contact, the transport is effectively ohmic. As the top contact to n-GaN is also Ohmic, the diodic response stems from affinity differences between the MgO high-k

oxide and the GaN semiconductor. The series resistance can also be obtained from the differential resistance through its proportionality to the current according to

$$\frac{dV}{dI} = \left(R_s + \frac{kT}{q} \left[\frac{1/I_0}{I/I_0 - 1} \right] \right) \approx R_s + \frac{nkT}{qI} \qquad (2)$$

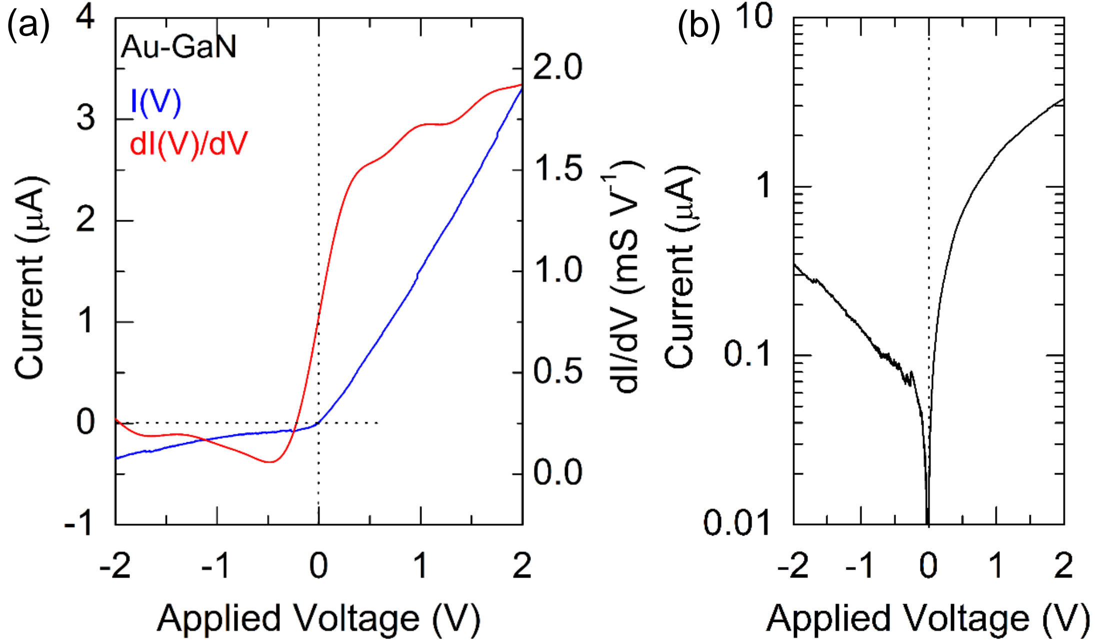

Figure 7. (a) *I*-*V* and d*I*/d*V* curves for Au-seeded porous n-GaN with a MgO dielectric layer. (b) ln(*I*)-*V* curve for the diode.

Figure 8a shows the differential resistance d*V*/d*I* as a function of applied of the inverse of the current in the high current region, plotted according to Eq. 2. Although it does not take account of specific grain boundary effects, the series resistance is estimated to be in the range 5-6 kΩ for the MgO/porous GaN sandwich. For the transport through the MgO/porous n-GaN stack, d*V*/d*I* approaches R_S at the higher currents, but as seen in Fig. 8b, the series resistance also includes likely tunnelling effects as the ideality factor is strongly voltage dependent and quite high in the higher current and higher bias regions. Further work is underway to identify mechanism contributing to such high ideality factors which in Schottky junctions are indicative of several mechanisms including tunnelling current, through multiple heterojunctions. Porosity complicates the transport mechanism, increasing shunt and series resistances (21).

Charge transport measurements through this system were conducted using 2- and 4-probe measurements and confirm the fabrication of a porous GaN diode with an *in-situ* grown crystalline MgO high-k dielectric layer. For Au-seeded porous n-GaN, Ohmic transport is found in the absence of a second oxide semiconducting layer between the intermetallic and the porous n-GaN, as shown in Figs 3 and 4. Further work is in progress to determine the direct effect of porosity on the reverse bias current mechanisms, and optimization of the diode response from Pt-seeded intermetallic-mediated porous GaN growth based on detailed investigations of the influence of the porosity on contact and sheet resistivity, and performance as a chemically inert, high surface area field effect transistor for sensing.

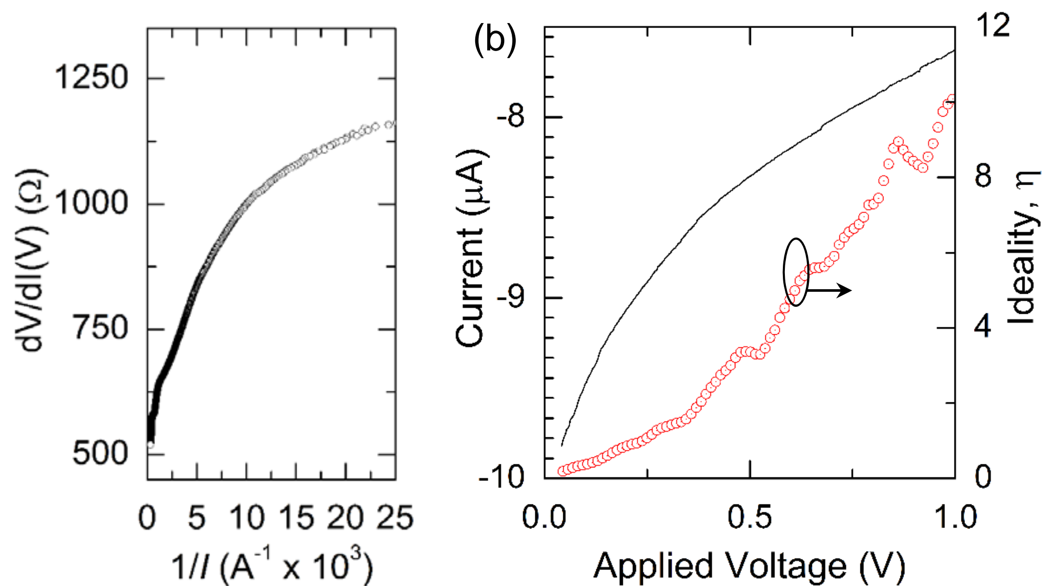

Figure 8. (a) Differential resistance (d*V*/d*I*) as a function of current for the MgO/porous GaN diode. (b) ln(*I*)-*V* curve and the voltage dependence of the ideality factor for the diode.

Conclusions

In summary, porous GaN particles have been successfully grown as high surface area layers from Pt- and Au-coated silicon substrates by a vapor-solid-solid process. The particles form as a layer of single-crystal particles with interparticle and intraparticle porosity. Current-voltage and capacitance-voltage measurements show near-ohmic transport through low-doped, polycrystalline (as a layer), porous n-GaN without alloy contacts or low work function metals. Metal-Ga intermetallic alloy formation during vapor-solid-solid growth promotes thermionic emission-based low-resistance ohmic transport through the porous layer and very low contact resistivity is possible to the faceted, rough n-GaN surface. By depositing Mg in a manner similar to deterministic p-type doping of GaN, a thin Mg films that is oxidized to polycrystalline MgO, is formed underneath the porous n-GaN layer, resulting in a high-k dielectric oxide that allows the single step formation of a porous GaN/MgO diode.

Acknowledgements

This work was supported by the EU Framework 7 under Project No. FP7-SPA-2010-263044, the Spanish Government under Projects No. MAT2011-29255-C02-02, TEC2010-21574-C02-02, PI09/90527, and by Catalan Authority under Project No. 2009SGR235. This work was also supported by Science Foundation Ireland under contract No. 07/SK/B1232a.

References

[1] S. Nakamura, S. Pearton, G. Fasol, G., *The Blue Diode Laser - The Complete Story*, Springer, Berlin, 7 (2000).

[2] A. Ramizy, Z. Hassan, K. Omar, *Sens. Actuators, B* **155**, 699 (2011).

[3] C. F. Lin, K. T. Chen, C. M. Lin, C. C. Yang, *IEEE Electron Dev. Lett.* **30**, 1057 (2009).

[4] M. Mynbaeva, A. Titkov, A. Kryganovskii, V. Ratnikov, K. Mynbaev, H. Huhtinen, R. Laiho, V. Dmitriev, *Appl. Phys. Lett.* **76,** 1113 (2000).

[5] Y. D. Wang, S. J. Chua, M. S. Sander, P. Chen. S. Tripathy, C. G. Fonstad, *Appl. Phys. Lett.* **85,** 816 (2004).

[6] S. Y. Bae, H. W. Seo, J. Park, H. Yang, B. Kim, *Chem. Phys. Lett.* **376,** 445 (2003).

[7] D. J. Diaz, T. L. Williamson, I. Adesida, P. W. Bohn, R. J. Molnar, *J. Appl. Phys.* **94**, 7526 (2003).

[8] R. S. Wagner, W. C. Ellis, *Appl. Phys. Lett.* **4**, 89 (1964).

[9] A. I. Persson, M. W. Larsson, S. Stenstron, B. J. Ohlsson, L. Samuelson, L. R. Wallenberg, *Nat. Mater.* **3**, 677 (2004).

[10] J. J. Carvajal, J. C. Rojo, *Cryst. Growth Des.* **9**, 320 (2009).

[11] J. J. Carvajal, O. V. Bilousov, D. Drouin. M. Aguiló, F. Díaz, J. C. Rojo, *Microsc. Microanal.* **18**, 1 (2012).

[12] C. O'Dwyer, M. Szachowicz, G. V. Visimberga, V. Lavayen, S. B. Newcomb, C. M. Sotomayor Torres, *Nat. Nanotech.* **4**, 239 (2009).

[13] C. O'Dwyer, D. N. Buckley, D. Sutton, S. B. Newcomb, *J. Electrochem. Soc.* **153**, G1039 (2006).

[14] M. E. Lin, Z. Ma, F. Y. Huang, Z. F. Fan, L. H. Allen, H. Morkoç, *Appl. Phys. Lett.* **64**, 1003 (1994).

[15] D. K. Schroder, *Semiconductor Material and Device Characterization*, Wiley, New York, 156 (1998).

[16] R. Sporken, C. Silien, F. Malengreau, K. Grigorov, R. Caudano, F. J. Sanchez, E. Calleja, E. Munoz, B. Beaumont, P. Gibart, *MRS Internet J. Nitride Semicond. Res.* **2**, 23 (1997).

[17] Yu. A. Goldberg, E. A. Posse, *Semiconductors,* **32**, 181 (1998).

[18] O. V. Bilousov, J. J. Carvajal, D. Drouin, X. Mateos, F. Díaz, M. Aguiló and C. O'Dwyer, *ACS Appl. Mater. Interfaces*, **4**, 6927 (2012).

[19] R. H. Horng, D. S. Wuu, Y. C. Lien, W. H. Lan, *Appl. Phys. Lett* **79,** 2925 (2001).

[20] D. J. Dumin, G. L. Pearson, *J. Appl. Phys.* **36**, 3418 (1965).

[21] G. Franssen, E. Litwin-Staszewska, R. Piotrzkowski, T. Suski, P. Perlin, *J. Appl. Phys.* **9**, 6122 (2003).